Physica E: Low-dimensional Systems and Nanostructures 114 (2019) 113619

Contents lists available at ScienceDirect

Physica E: Low-dimensional Systems and Nanostructures

journal homepage: www.elsevier.com/locate/physe

Thermoelectric properties of low-cost transparent single wall carbon nanotube thin films obtained by vacuum filtration

Igor A. Tambasov[a,*], Anton S. Voronin[b], Natalia P. Evsevskaya[a,c], Mikhail N. Volochaev[a], Yuri V. Fadeev[b], Mikhail M. Simunin[b,e], Aleksander S. Aleksandrovsky[a,e], Tatyana E. Smolyarova[b,e], Seryozha R. Abelian[a], Ekaterina V. Tambasova[d], Maxim O. Gornakov[a], Valentina A. Eremina[f,g], Yuri M. Kuznetsov[h], Mikhail V. Dorokhin[h], Elena D. Obraztsova[f,g]

[a] Kirensky Institute of Physics, Federal Research Center KSC Siberian Branch of Russian Academy of Sciences, Akademgorodok 50, 660036 Krasnoyarsk, Russia
[b] Krasnoyarsk Scientific Center, Federal Research Center KSC Siberian Branch of Russian Academy of Sciences, Akademgorodok 50, 660036 Krasnoyarsk, Russia
[c] Institute of Chemistry and Chemical Technology, Federal Research Center KSC Siberian Branch of Russian Academy of Sciences, Akademgorodok 50, 660036 Krasnoyarsk, Russia
[d] Reshetnev Siberian State University of Sciences and Technologies, Krasnoyarsky Rabochy Avenue 31, 660037 Krasnoyarsk, Russia
[e] Siberian Federal University, Svobodny Avenue 79, 660041 Krasnoyarsk, Russia
[f] Prokhorov General Physics Institute of RAS, Vavilov Street 38, 119991 Moscow, Russia
[g] Moscow Institute of Physics and Technology, 141701, Institutskiy per.9, Dolgoprudny, Moscow Region, Russia
[h] Lobachevsky State University of Nizhny Novgorod, Gagarin Avenue 23/3, 603950 Nizhny Novgorod, Russia

ARTICLE INFO

Keywords:
Single-wall carbon nanotubes
Aqueous two-phase extraction
Semiconducting and metallic SWNTs
Thin SWNT films
Thermoelectric properties
Thermoelectric figure of merit

ABSTRACT

The dispersions of semiconducting (*sc*-) and metallic (*m*-) SWCNTs with purity more than 98 and 86%, correspondingly, were obtained by using the aqueous two-phase extraction method. The unseparated (*un*-) SWCNTs contained ~3/4 of semiconducting and ~1/4 of metallic nanotubes. Thin films based on unseparated, semiconducting and metallic SWCNTs were prepared by vacuum filtration method. An Atomic Force Microscopy (AFM) and a Transmission Electronic Microscopy (TEM) were used to investigate the thin film microstructure. The thin SWCNT film transmittance was measured in the wavelength range of 300–1500 nm. Thermoelectric properties were carried out in the temperature range up to 200 °C. The largest Seebeck coefficient was observed for thin films based on semiconducting SWCNTs. The maximum value was 98 μV/K under the temperature of 170 °C. The lowest resistivity was $7.5{\cdot}10^{-4}$·Ohm·cm at room temperature for thin *un*-SWCNT films. The power factor for *m*-SWCNT and *un*-SWCNT films was 47 and 213 $\mu W\,m^{-1}\,K^{-2}$, correspondingly, at room temperature and 74 and 54 $\mu W\,m^{-1}\,K^{-2}$ at 200 °C, respectively. For a thin *sc*-SWCNT film the maximum power factor was 2.8 $\mu W\,m^{-1}\,K^{-2}$ at 160 °C. The *un*-SWCNT film thermal conductivity coefficient was 5.63 and 3.64 $W\,m^{-1}\,K^{-1}$ and a thermoelectric figure of merit was 0.011 and 0.016 at temperatures of 23 and 50 °C, respectively.

1. Introduction

A huge part of unused thermal energy from industrial production and other areas of human activity is dispersed into the environment. A part of this thermal energy can be converted into electrical energy by using thermoelectric converters. The most significant part of unused thermal energy is in the range of temperatures up to 200 °C [1].

For efficient conversion of thermal energy into electrical, materials with high thermoelectric properties are needed. The key properties are a high hole or electron conductivity σ ($S{\cdot}m^{-1}$), a high Seebeck coefficient S ($V{\cdot}K^{-1}$) and a lowest thermal conductivity coefficient κ ($W{\cdot}m^{-1}{\cdot}K^{-1}$) [2]. A general integral characteristic of thermoelectric materials is a thermoelectric figure of merit $ZT = (S^2\sigma/\kappa)T$, where T is the average temperature between the hot and cold sides of a thermoelectric converter.

Nanostructured materials have a big potential to demonstrate a high thermoelectric figure of merit [3–6]. On the one hand, this is because the additional scattering centers of thermal phonons can be realized on nanoscale structures [7–9]. This leads to an effective reduction of thermal conductivity. On the other hand, the energy filtration of charge carriers can also be implemented on a nanostructured materials [10–13]. The energy filtering is realized due to the effective scattering

* Corresponding author.
E-mail address: tambasov_igor@mail.ru (I.A. Tambasov).

https://doi.org/10.1016/j.physe.2019.113619
Received 7 March 2019; Received in revised form 21 June 2019; Accepted 23 June 2019
Available online 29 June 2019
1386-9477/

of low energy electrons. These electrons significantly reduce the Seebeck coefficient. This scattering can occurs on ground boundary when the electrons have energies less than the barrier height. As a result, the contribution of low energy electrons to transport properties is minimized and the coefficient Seebeck increases [14]. Thus, new nanostructured thermoelectric materials may significantly improve the thermoelectric figure of merit.

The nanostructured materials based on single-wall carbon nanotubes (SWCNTs) [15] and nanocomposites based on them [16,17] are very promising for thermoelectric applications. This is because a high value of Seebeck coefficient was found for semiconducting single-walled carbon nanotubes [18]. Worth noting that materials based on SWCNTs concede in their thermoelectric properties to traditional materials based on bismuth and tellurium [19]. However, SWCNTs are suitable to create flexible nanocomposite thermoelectrics [17]. Moreover, thin SWCNT films were reported to have thermoelectric properties combined with an optical transparency [15]. Thus, it is possible to implement several functional properties such as flexibility, optical transparency and thermoelectric properties within one material. Thin films based on SWCNTs can be used for transparent flexible electronics as power sources positioned on a transparent carrier [20].

The Seebeck coefficient and electrical conductivity of thin SWCNTs films strongly depend on semiconducting and metallic fraction ratio of used SWCNTs [18,21–23]. In most cases, 2/3 of semiconducting and 1/3 of metallic fractions are obtained by nanotube synthesis [24]. Also, the semiconducting SWCNT fraction is preferably to be used to improve the Seebeck coefficient. For this purpose, several methods have been developed to separate nanotubes into metallic and semiconducting fractions from parent SWCNTs [25–29]. There is also a simple and highly efficient SWCNT separation based on aqueous two-phase extraction (ATPE) [28,30,31]. From the point of view of practical application, industrially accessible SWCNTs should be used to minimize costs of thermoelectric materials. Thus, a study associated with the simple separation of industrially accessible SWCNTs and formation on their basis of thermoelectric materials, as well as a thermoelectric property research are the actual applied problems.

In the present study, we have separated industrially accessible SWCNTs into semiconducting and metallic fractions by using aqueous two-phase extraction. In addition, thin films based on unseparated, semiconducting and metallic SWCNTs were obtained by vacuum filtration. The microstructure, optical transmittance and thermoelectric properties of thin films were investigated.

2. Experimental

2.1. Preparation of dispersions and separation of SWCNTs

The dry raw materials of SWCNTs (Tuball) was purchased from OCSiAl company (Novosibirsk, Russia). To prepare aqueous two-phase system for extraction, dextran DX 70 kDa (AppliChem), PEG 6 kDa (Panreac), sodium dodecyl sulfate (SDS, Panreac) and sodium cholate (SC, Bio chemical) were purchased. During this work, we selected the optimal preparation mode for the dispersion of Tuball SWCNTs. It was necessary to disperse SWCNT dry raw material 1mg/1 ml in a 2% SC solution by using a tip ultrasonication (power 10 W/ml during 3 h) and centrifuging under 70.000 rpm during 1 h.

The solutions of polymers and surfactants were prepared by dissolving the appropriate amounts of substances in distilled water. Aqueous solutions of polymers DX 20% and PEG 50% were mixed in a given proportion. The surfactants (SC 10%, SDS 10%) and the Tuball dispersion were added in aqueous solutions of polymers. All components were mixed in closed tubes for a few seconds and left until the spontaneous separation of the components into two phases. Phases with separated SWCNTs were selected by a simple pipetting. Thereafter, dispersions with semiconducting or metallic SWCNTs were transfused into quartz cuvettes (quartz grade KU-1, volume 0.7 ml, optical path length 10 mm) to measure optical absorption by a Shimadzu UV-3600 spectrometer. It is worth noting that a main tool for determining dispersions with metallic or semiconducting single-walled carbon nanotubes is optical absorption [32].

2.2. Fabrication of thin SWCNT films

Thin films based on unseparated, semiconducting and metallic of SWCNTs were fabricated by using vacuum filtration. This method allowed lossless production of thin films from a dispersion small amount of unseparated and separated SWCNTs. The thickness of thin films was set by the volume of the dispersion of single-walled carbon nanotubes used for vacuum filtration. The corresponding nanotube dispersion volumes (20 μl - 300 μl) were diluted in distilled water to a volume of 30–250 ml. The resulting solution was filtered through the acetate cellulose filters with vacuum pumping. A pore diameter was 600 nm. Thin SWCNT film was formed on the filter surface. The choice of filter was based on the possibility of its further removal by dissolving in acetone without loss of SWCNT films. The wet SWCNT film on the filter was tightly pressed to a glass (PET) substrate by means of a clamp. The SWCNT film on the glass substrate was dried at 80 °C. Next, the SWCNT film on the carrier substrate was placed in a container with acetone. To remove completely the filter residues, it was necessary to replace the solvent at least five times and rinse it with a deionized water. In conclusion, it was necessary to perform annealing at 450 °C in a nitrogen atmosphere. The annealing temperature in a nitrogen atmosphere was decreased to 100 °C when using a PET substrate.

2.3. Characterization of thin SWCNT films

The surface morphology of thin films was determined using an atomic-force microscope Nanoink DPN 5000. To assess the microstructure and thickness of thin SWCNTs films, a cross section of the film was used [33–35]. The cross section of the thin films were received by Hitachi TM7700 transmission electron microscope (TEM). For this purpose, cross-sectional TEM specimens were prepared by a focused ion beam of 40 keV Ga^+ beam system (FIB) Hitachi FB-2100 with follow final ion milling (Ar^+ 2 kV) to reduce the specimens thickness below 40 nm. A Ge protective layer was selected and formed by thermal deposition at room temperature. The using of this Ge layer is necessary to protect the thin SWCNT films from structural degradation during FIB preparation and to improve contrast in TEM images. The optical properties of thin SWCNT films were studied using a Shimadzu UV-3600 spectrometer.

Measurements of thin film thermoelectric properties (Seebeck coefficient and electrical resistivity) from room temperature to 200 °C were carried out with the home-made installation. The installation includes a thermostat, a Keithley 2400 precision current source, a specially designed sample holder, two K-type thermocouples and a 24-bit analog-to-digital converter LTR114 based on the LTR-EU-2 crate (L-CARD company, Russia). A detailed description of the installation can be found in Ref. [15]. The silver contact pads were made using an Emitech k575x vacuum unit. The contact thickness was ~500 nm. 2-probe circuit was used to measure electrical resistivity.

Measurement of thermal conductivity in thin films was carried out using 3 Ω method. For this purpose, a golden narrow strip on thin SWCNT films was produced using optical lithography. The length and width of the strip were 3000 and 20 μm, respectively. The golden stripe resistance was 268 Ohm. A detailed description of the 3 Ω method can be found in the articles [36–39].

3. Results and discussion

3.1. Separation and formation of thin films based on SWCNTs

During the work, the volume ratio of surfactants was found to

Table 1
The reactant ratio for the experiment series A and B.

№ experiment	DX 20%, ml	PEG 50%, ml	SC 10%, ml	SDS10%, ml	SWCNTs в 2% SC, ml
A1	1.6	0.73	0.3	0.1	1.2
A2				0.2	
A3				0.3	
A4				0.4	
B1			0.1	0.3	
B2			0.2		
B3			0.3		
B4			0.4		

influence greatly on the separation. In experimental series A, SC volume remained constant and SDS volume was increased in each experiment. With a lack of SDS, the SWCNTs are extracted to the lower dextran phase (bottom). A separation was observed when the ratio reaches SC: SDS = 0.3: 0.3 (experiment A3). The metallic tubes preferentially pass into the dextran lower phase, while semiconducting ones pass into the PEG upper phase (top). With a further increase in the SDS content, the SWCNTs are extracted into the PEG upper phase (experiment A4).

In a similar experimental series B, SDS volume remained constant and SC volume was increased in each experiment. A similar pattern is observed. With a lack of SC, nanotubes are extracted into the PEG upper phase. With an equal ratio SC: SDS = 0.3: 0.3, the separation of metallic and semiconducting SWCNTs was observed. The SWCNT extraction occurred into the dextran lower phase at a SC excess. Detailed quantitative ratios of the used reagents are shown in Table 1.

Images of the corresponding SWCNT dispersions at reactant different ratios, as well as their optical absorption are presented in Fig. 1.

Thus, it is possible to control the separation process by varying the surfactant ratio. With this approach, the dispersions with a high degree of separation or mixed dispersions with a controlled content of semiconducting and metallic nanotubes can be obtained.

In course of research, it was found that the metallic SWCNT concentration increases when the reagents pre-cooled down to 10 °C were used. It is explained by a diffuse factor decrease under the lower temperature. The nanotubes are concentrated at the interface primarily while the room temperature reagents are used. This leads to a decrease of SWCNT concentration in the polymer phase. Fig. 2 shows the

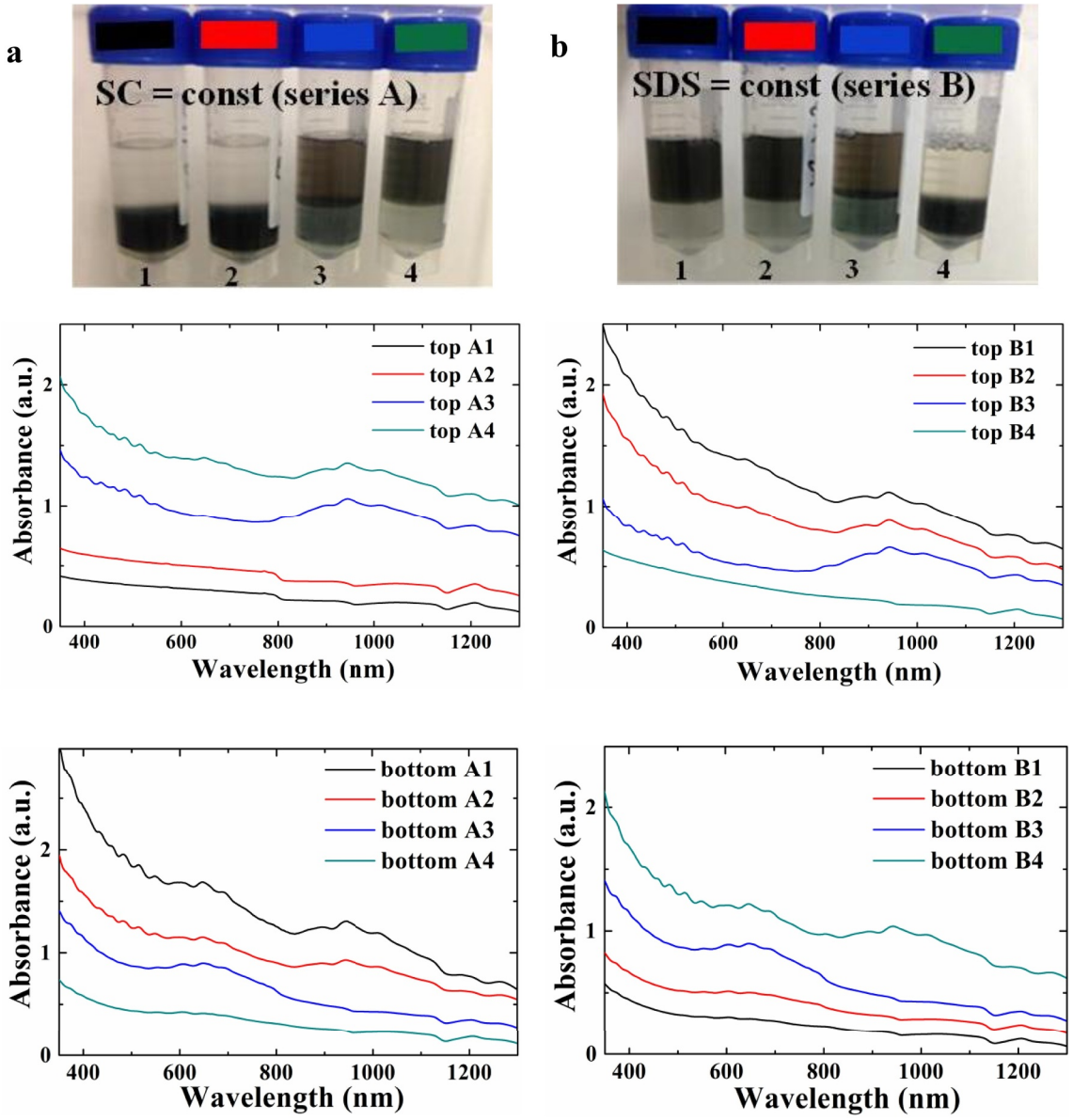

Fig. 1. Appearance and optical absorption spectra of SWCNT dispersions obtained by two-phase aqueous extraction for the experiment series A (a) and B (b).

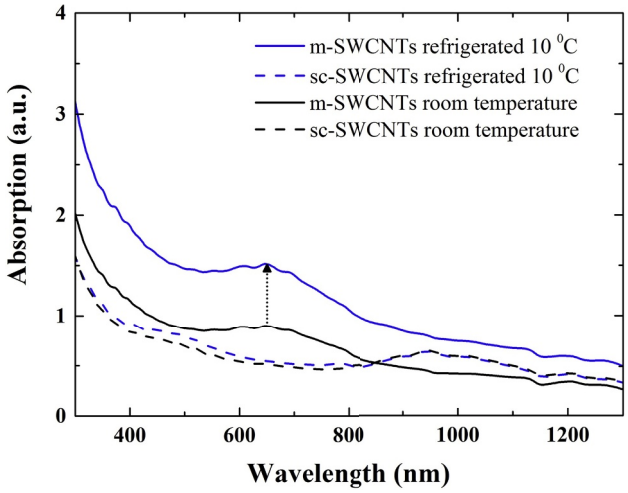

Fig. 2. Absorption as a function of wavelength for separated over conductivity type SWCNT dispersions produced at room temperature and at 10 °C.

absorption spectra of SWCNT dispersions enriched with semiconducting or metallic fractions.

As it can be seen from Fig. 2, the cooling reactant effect is more visible for metallic SWCNTs.

The degree of semiconducting $Y^{s\text{-}SWCNT}$ and metallic $Y^{m\text{-}SWCNT}$ nanotube separation was estimated by analyzing the optical absorption spectra. The main control method is optical spectrophotometry [32,40]. The measurements were carried out in range 200–1300 nm. In this range, peaks S_{22} and S_{33} characterizing semiconducting SWCNTs and M_{11} peak corresponding metallic nanotubes are clearly distinguishable. The measurement was carried out in quartz cuvettes (quartz grade KU-1). The cuvette volume was 0.7 ml and the optical path length was 10 mm. Fig. 3 shows the absorption spectra of unseparated, semiconducting and metallic SWCNT dispersions obtained in experiment A3.

From Fig. 3, the estimations of unseparated, semiconducting and metallic SWCNT purity were made by using the following expressions 1–2:

$$Y^{s-SWCNT} = \frac{A_{S22}}{(A_{S22} + A_{M11})} \quad (1)$$

$$Y^{m-SWCNT} = \frac{A_{M11}}{(A_{S22} + A_{M11})}, \quad (2)$$

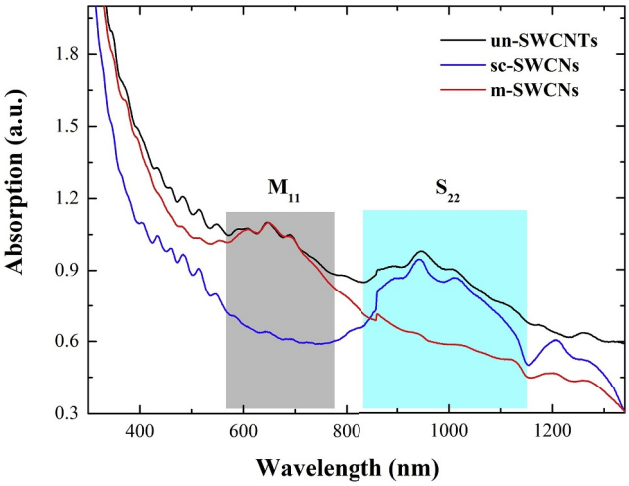

Fig. 3. Optical absorption of dispersions from unseparated, semiconducting and metallic single-walled carbon nanotubes, obtained in experiment A3.

where A_{S22}, A_{M11} are the peak areas corresponding to the second and first Van Hove singularities for semiconducting and metallic SWCNTs, respectively.

The best results were obtained in experiment A3 and B3, which are completely similar. The purity of the metallic SWCNTs was more than 86% and the purity of semiconducting SWCNTs was more than 98%. It was found that unseparated SWCNTs (Tuball) consist of ~3/4 of semiconducting and ~1/4 of metallic fractions. This ratio is 2/3 and 1/3 for semiconducting and metallic nanotubes for many methods of synthesizing SWCNTs.

The complete process of thin SWCNT film formation by vacuum filtration is shown in Fig. 4.

Vacuum filtration is a simple method for producing thin films from a small amount of SWCNT dispersions.

Fig. 5a shows the images of unseparated SWCNT dispersions.

As it can be seen from Fig. 5b–d, thin films based on single-walled carbon nanotubes can be formed both on glass and on PET substrates by vacuum filtration.

3.2. Structural and optical properties of thin SWCNT films

To study the thin film morphology, we used an atomic force microscopy. The surfaces of thin films based on unseparated, semiconducting and metallic SWCNTs were investigated as shown in Fig. 6a–c.

Fig. 6a–c shows that the thin film morphology is a branched surface based on SWCNTs. In addition, there is a number of tube bundles.

Microscopic studies of thin films based on SWCNTs were carried out using transmission electron microscopy. Typical thin SWCNT film microstructures are shown in Fig. 7a–b.

It can be seen from Fig. 7a that a thin film was non-uniform in thickness. In addition, it is clear that the SWCNTs were chaotically arranged along the film thickness (see Fig. 7b.). Fig. 7b also shows the cross sections of individual tubes. This allowed us to estimate the nanotube diameter, which was equal ~1.7–1.9 nm. This diameter value is in a good agreement with our previous results, which were obtained by Raman spectroscopy [15].

Materials based on various allotropic forms of carbon are known to absorb effectively light in a wide spectral range [41,42]. For this reason, we have performed the optical transmittance studies in the visible spectral range for thin films based on unseparated SWCNTs with various thicknesses. Fig. 8a shows the transmittance dependence on the wavelength for thin SWCNT films.

The optical transmittance decreased throughout the spectrum with increasing the SWCNT film thickness as can be seen in Fig. 8a. Fig. 8b shows the transmittance dependence on the film thickness at 550 nm considering the substrate transmittance. This dependence is almost linear. The transmittance dependences on the wavelength for thin films based on semiconducting and metallic SWCNTs are presented in Fig. 8c. Only characteristic feature S_{22} was visible for the thin *sc*-SWCNT film. On the other hand, more pronounced characteristic feature M_{11} and less pronounced characteristic feature S_{22} were observed for the thin *m*-SWCNT film. Probably, the metallic SWCNT dispersion contained a small amount of semiconducting fraction.

3.3. Thermoelectric properties of thin SWCNT films

First, we have conducted a measurement series of the Seebeck coefficient and the resistivity ρ of thin films based on unseparated SWCNTs. These measurements were carried out in the temperature range up to 200 °C. The Seebeck coefficient temperature dependence was similar for all thin films based on unseparated SWCNTs. Fig. 9a shows the Seebeck coefficient temperature dependence for thin films based on unseparated, semiconducting and metallic single-walled carbon nanotubes.

As it can be seen from Fig. 9a, the largest Seebeck coefficient was

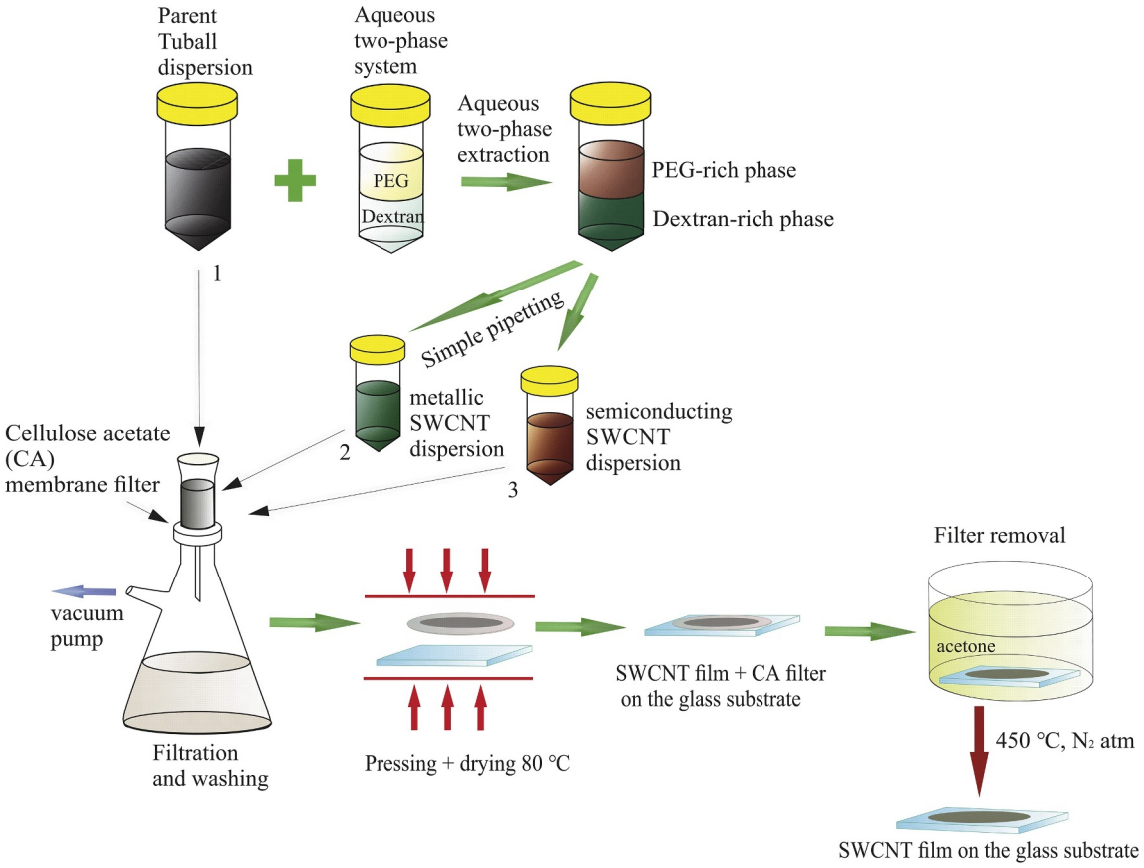

Fig. 4. A block diagram of the process of thin SWCNT film formation on glass substrates.

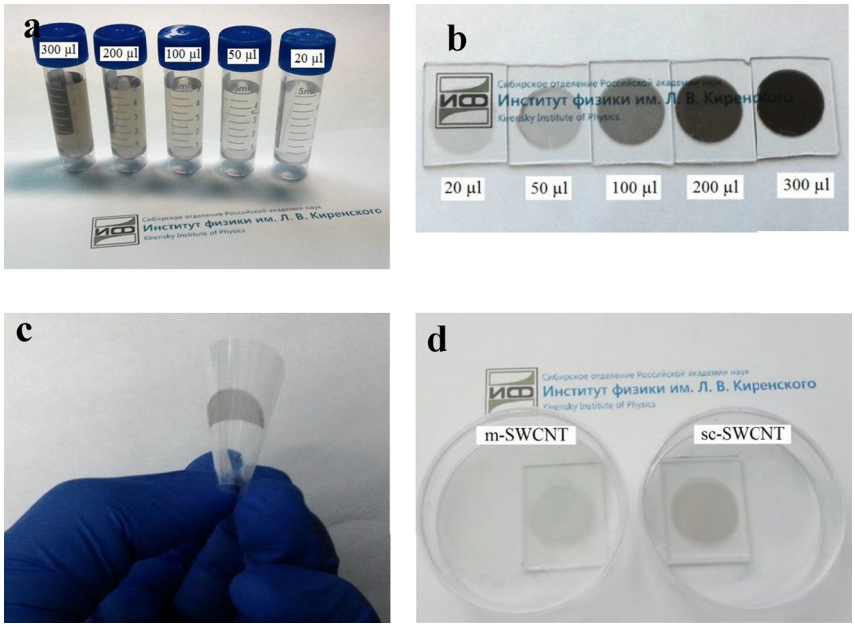

Fig. 5. A view of initial dispersions of unseparated SWCNTs (a), thin films obtained from unseparated SWCNTs by vacuum filtration on glass (b) and PET (c). The images of thin films based on metallic and semiconducting single-walled carbon nanotubes (d) on glass.

observed for thin films based on semiconducting SWCNTs. In addition, the maximum Seebeck coefficient was 98 µV/K at a temperature of 170 °C. This value of the Seebeck coefficient is typical for thin *sc*-SWCNT films [40,43]. The Seebeck coefficient for thin films based on unseparated and metallic SWCNTs are relatively similar. In most research, it was shown that the Seebeck coefficient of thin *m*-SWCNT films was less than for thin *un*-SWCNT films [18,40]. However, we observed a slight increase in the Seebeck coefficient for thin *m*-SWCNT films relative to that of thin *un*-SWCNT films. We assume that it happens for the following reason. To significantly reduce the thin *m*-SWCNT film resistivity, a removal of dextran from metallic SWCNT dispersion was made using ultrasound and boiling with acetic acid. It is

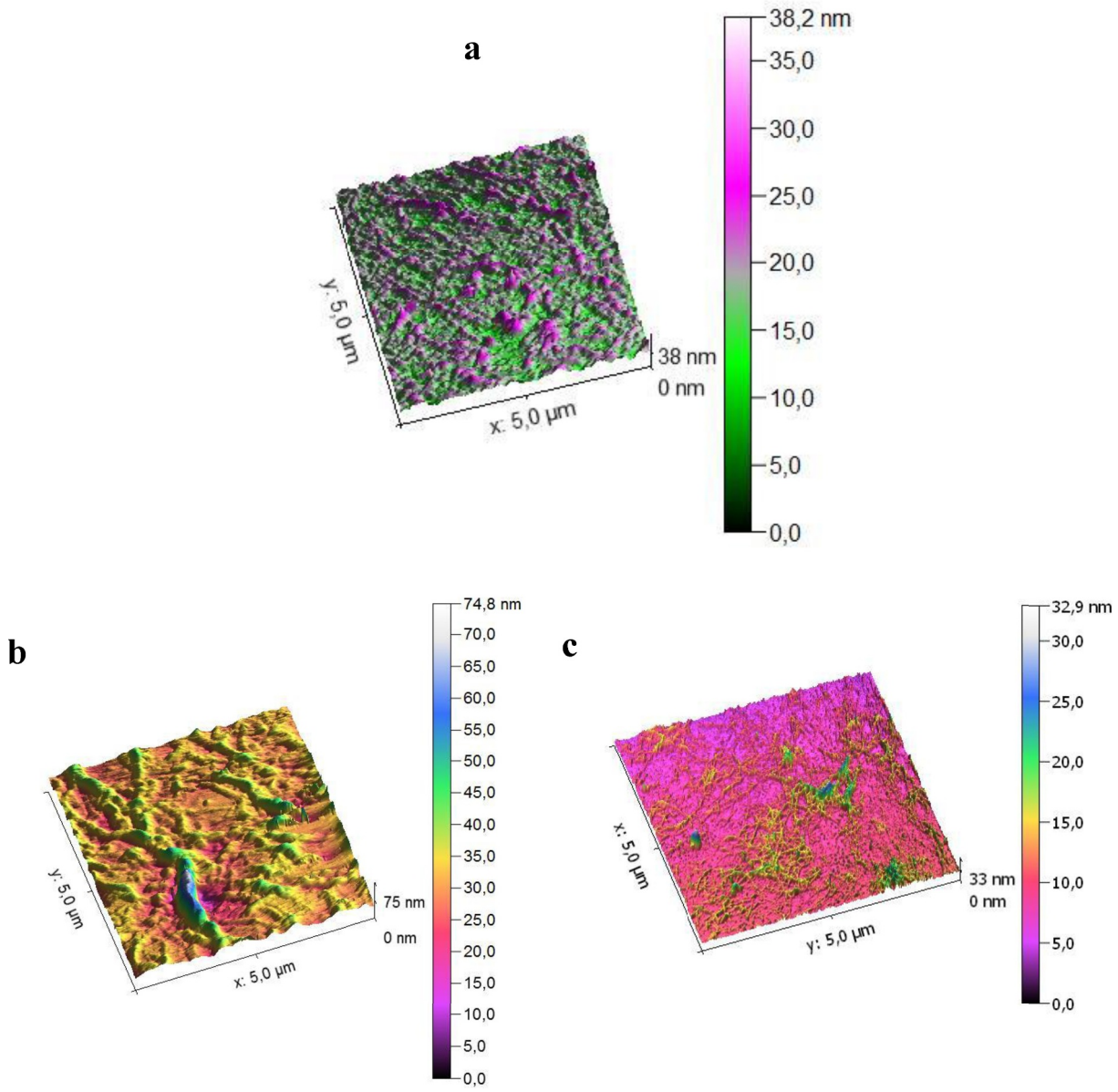

Fig. 6. AFM images of thin films based on unseparated (a), metallic (b) and semiconducting (c) SWCNTs.

possible that such processing can modifies electronic structure of metallic SWCNTs [44]. An adsorption of acetic acid molecules creates additional SWCNT surface COOH groups [45], which can be considered as an acceptor impurity [46]. Thus, the electronic structure of metallic SWCNT is changing and it is possible that this leads to increase of the Seebeck coefficient.

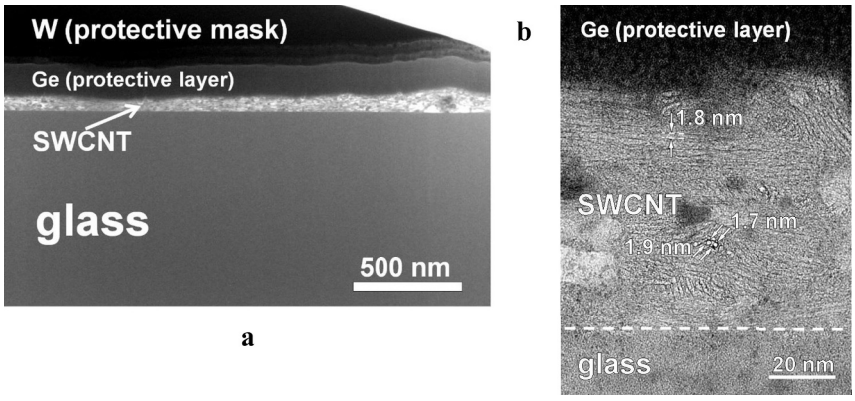

Fig. 7. Overview (a) and the high-resolution (b) TEM images of 65 nm thin film based on unseparated SWCNTs.

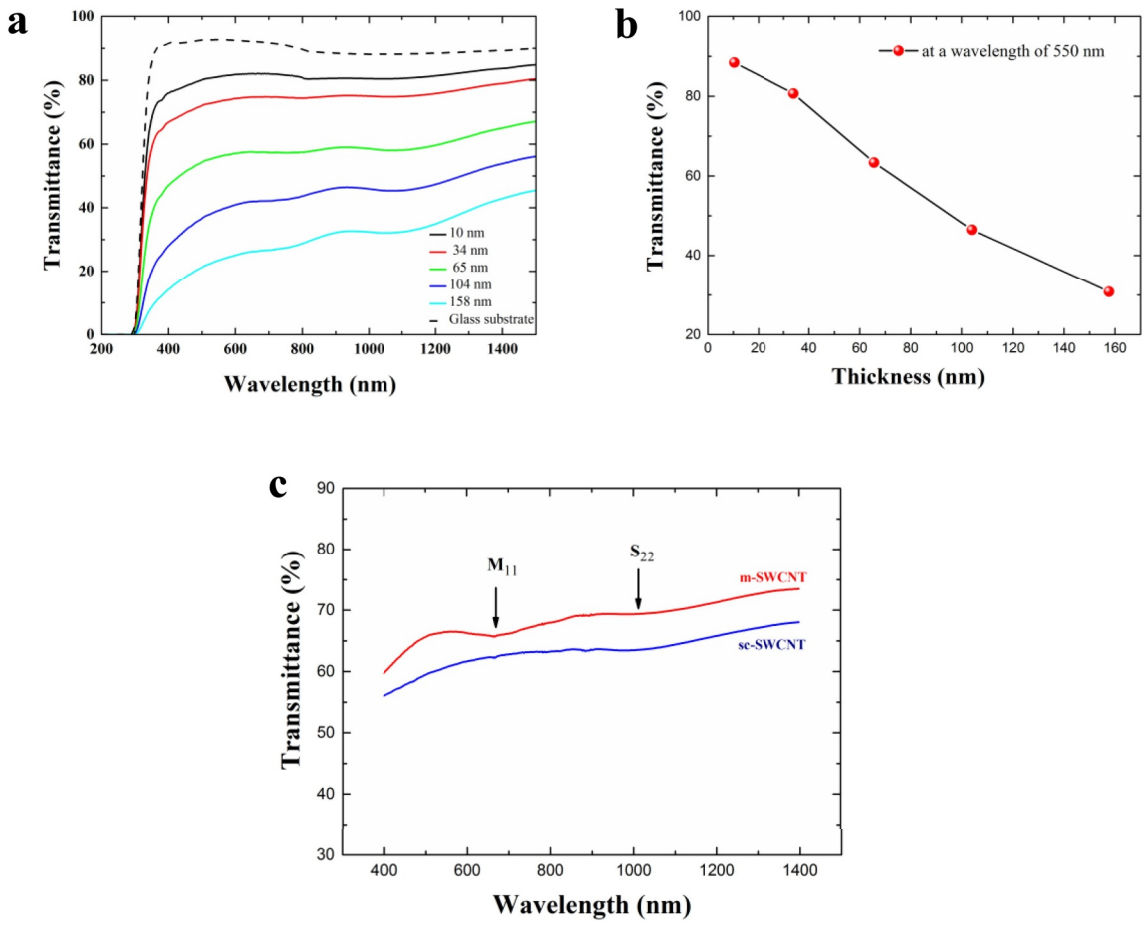

Fig. 8. The transmittance dependence on the wavelength for thin films based on unseparated SWCNTs (a). The dependence of transmittance on the film thickness at 550 nm (b). The transmittance dependence on the wavelength for thin 27 nm semiconducting and 25 nm metallic SWCNT films (c).

Fig. 9b shows the resistivity temperature dependences for thin films based on unseparated, semiconducting, and metallic SWCNTs. It is worth noting here that the resistivity temperature dependence for thin films based on unseparated SWCNTs is the same for all samples. Thin SWCNT films represent a porous structure consisting of numerous nanotubes, which create numerous bundles. Moreover, there is contact resistance between nanotubes. This contact resistance is dominant for total resistance of thin SWCNT films. For this reason, the transport depending on temperature can be complicated in thin SWCNT films [47]. Similar temperature dependence of thin SWCNT film resistivity was observed experimentally [40,48–50]. Thin *un*-SWCNT film demonstrates lowest resistivity, as can be seen from Fig. 9b. The lowest resistivity was $7.5{\cdot}10^{-4}$·Ohm·cm at room temperature. A relatively high resistivity for *s*-SWCNT and *m*- SWCNT thin films primarily associated with the polymer (DX and PEG) residues after the separation process. The additional reason could be the SWCNT length decrease in the process of thin film form. To form thin films from metallic or semiconducting SWCNT dispersions, an additional ultrasonic processing is used, i.e. processing time increases. With increasing ultrasonic processing time, SWCNT length decrease as shown by experimental studies [51,52]. As a result, the thin film resistivity based on separated SWCNTs is higher.

One of the important integral characteristics of thermoelectric materials is the power factor *PF* (μW·m^{-1}·K^{-2}), which is determined by the following expression 3:

$$PF = S^2\sigma \quad (3)$$

We used expression 3 to construct the power factor temperature dependence for 34 nm thin *un*-SWCNT film, 27 nm thin *sc*-SWCNT film and 25 nm thin *m*-SWCNT film as shown in Fig. 8c. To do this, we recalculated electrical conductivity through resistivity as $\sigma = 1/\rho$. Fig. 9c shows that the power factor for a thin *un*-SWCNT film at room temperature was much higher than for *sc*-SWCNT and *m*-SWCNT films. The power factor for a thin *un*-SWCNT film was 213 μW m^{-1} K^{-2} at room temperature. However, the power factor decreased as the temperature increased and was 54 μW m^{-1} K^{-2} at the temperature of 200 °C. On the other hand, the power factor for thin *m*-SWCNT film was 47 and 74 μW m^{-1} K^{-2} at room temperature and 200 °C, respectively. The maximum power factor for a thin *sc*-SWCNT film was 2.8 μW m^{-1} K^{-2} at 160 °C. Thus, from the point of view of thermoelectric properties, thin *un*-SWCNT films are more preferable due to their high electrical conductivity. It is possible that the use of more advanced methods of SWCNT separation could provide a significantly higher power factor in thin *sc*- SWCNT films.

In order to estimate the thermoelectric figure of merit in thin *un*-SWCNT films, which are more preferable from point of view of their thermoelectric properties, we carried out measurements of the thermal conductivity coefficient using the 3 Ω method. The measurements were carried out at temperatures of 23 and 50 °C. The power factor has relatively high values in this temperature range. The thermal conductivity coefficient was 5.63 and 3.64 W m^{-1} K^{-1} for 23 and 50 °C, respectively.

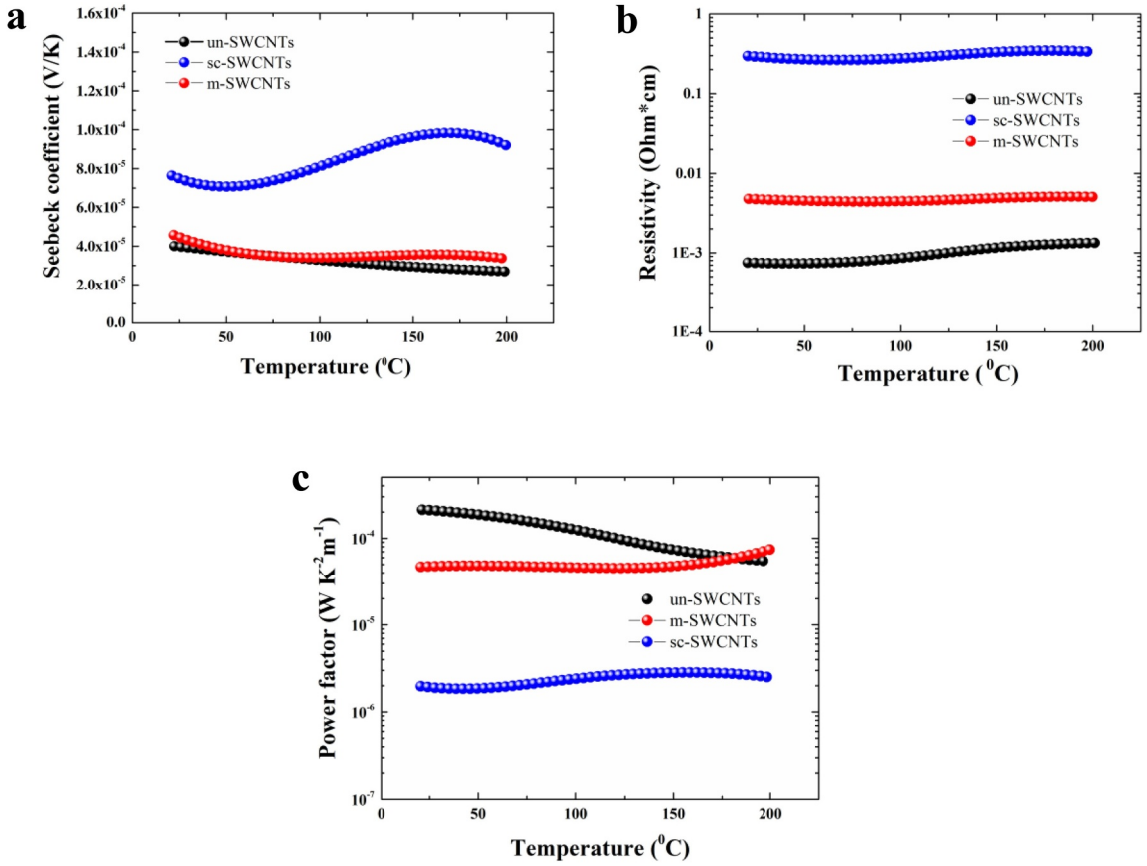

Fig. 9. The temperature dependence of the Seebeck coefficient (a), the resistivity (b) and the power factor (c) for 34 nm thin *un*-SWCNT film (black circles), 27 nm thin *sc*-SWCNT film (blue circles) and 25 nm thin *m*-SWCNT film (red circles). (For interpretation of the references to colour in this figure legend, the reader is referred to the Web version of this article.)

Such values of thermal conductivity coefficient are comparable to the values published in papers [43,53]. Thus, thermoelectric figure of merit for thin *un*-SWCNT films was 0.011 and 0.016 at temperatures of 23 and 50 °C, respectively. Our thin films have high thermoelectric properties in comparison with other thin films based on un-SWCNTs [16].

We believe that the thin films obtained from industrially available SWCNTs might become the basis for the manufacture of highly efficient thermoelectric nanocomposite materials.

4. Conclusion

In summary, dispersions based on unseparated, semiconducting and metallic SWCNTs from industrially available single-wall carbon nanotubes were obtained. The aqueous two-phase extraction method was used to obtain semiconducting and metallic SWCNT dispersions. It was found that unseparated SWCNTs (Tuball) consist of ~3/4 of semiconductor and ~1/4 of metal fractions. For SWCNTs, synthesized by many methods, this ratio is 2/3 and 1/3 for semiconducting and metallic nanotubes, respectively. This method allowed to obtain dispersions with the purity of semiconducting and metallic single-walled carbon nanotubes higher than 98 and 86%, respectively. It was found that it is possible to achieve the necessary ratio of semiconducting and metallic SWCNT fractions in the dispersion by varying the surfactant. Moreover, it was shown that the concentration of metallic SWCNTs increases while the reagents, pre-cooled down to 10 °C, were used.

Thin films based on unseparated, semiconducting and metallic SWCNTs were formed from the appropriate dispersions using vacuum filtration. Thin film surface was investigated by using an atomic force microscopy. The optical transmittance of thin SWCNT films was measured in the wavelength range of 300–1500 nm. Measurements of the Seebeck coefficient and the resistivity were carried out in the temperature range up to 200 °C. It was found that the largest Seebeck coefficient was observed for thin films based on semiconducting SWCNTs. The maximum Seebeck coefficient was 98 μV/K at the temperature of 170 °C. Thin *un*-SWCNT films had the lowest resistivity and was $7.5 \cdot 10^{-4}$·Ohm·cm at room temperature. The power factor for a thin *un*-SWCNT film was 213 $\mu W\,m^{-1}\,K^{-2}$ at room temperature. However, as the temperature increased, the power factor decreased down to 54 $\mu W\,m^{-1}\,K^{-2}$ at the temperature of 200 °C. On the other hand, the power factor for thin *m*-SWCNT film was 47 and 74 $\mu W\,m^{-1}\,K^{-2}$ at room temperature and 200 °C, respectively. The maximum power factor for a thin sc-SWCNT film was 2.8 $\mu W\,m^{-1}\,K^{-2}$ at 160 °C. Thus, from the point of view of thermoelectric properties, thin *un*-SWCNT films are more preferable due to a high electrical conductivity. For thin *un*-SWCNT films, the coefficient of thermal conductivity was 5.63 and 3.64 $W\,m^{-1}\,K^{-1}$ for 23 and 50 °C, respectively. The thermoelectric figure of merit was 0.011 and 0.016 at temperatures of 23 and 50 °C, respectively.

We believe that the thin films obtained from industrially available SWCNTs might become the basis for the manufacture of highly efficient thermoelectric nanocomposite materials.

Acknowledgments

The study was carried out by a grant of Russian Science Foundation (project No. 17-72-10079). The electron microscopy examination was carried out at the Center for Collective Use of the Krasnoyarsk Scientific Center of the Siberian Branch of the Russian Academy of Sciences (Krasnoyarsk, Russia). V.A.E. and E.D.O. thank RFFI-18-32-00998_mol_a and RFFI-19-02-00859_a projects for support of development of two aqueous phase technique for nanotube separation.

References

[1] N. Toshima, Recent progress of organic and hybrid thermoelectric materials, Synth. Met. 225 (2017) 3–21 https://doi.org/10.1016/j.synthmet.2016.12.017.
[2] G.J. Snyder, E.S. Toberer, Complex thermoelectric materials, Nat. Mater. 7 (2008) 105–114 https://doi.org/10.1038/nmat2090.
[3] J. Zhang, D. Wu, D.S. He, D. Feng, M.J. Yin, X.Y. Qin, J.Q. He, Extraordinary thermoelectric performance realized in n-type PbTe through multiphase nanostructure engineering, Adv. Mater. 29 (2017) 1703148 https://doi.org/10.1002/adma.201703148.
[4] X.L. Su, P. Wei, H. Li, W. Liu, Y.G. Yan, P. Li, C.Q. Su, C.J. Xie, W.Y. Zhao, P.C. Zhai, Q.J. Zhang, X.F. Tang, C. Uher, Multi-Scale microstructural thermoelectric materials: transport behavior, non-equilibrium preparation, and applications, Adv. Mater. 29 (2017) 1602013 https://doi.org/10.1002/Adma.201602013.
[5] J. He, T.M. Tritt, Advances in thermoelectric materials research: looking back and moving forward, Science 357 (2017) 1369 https://doi.org/10.1126/science.aak9997.
[6] J.F. Li, W.S. Liu, L.D. Zhao, M. Zhou, High-performance nanostructured thermoelectric materials, NPG Asia Mater. 2 (2010) 152–158 https://doi.org/10.1038/asiamat.2010.138.
[7] P. Pichanusakorn, P. Bandaru, Nanostructured thermoelectrics, Mater. Sci. Eng. R Rep. 67 (2010) 19–63 https://doi.org/10.1016/j.mser.2009.10.001.
[8] L. Yang, Z.G. Chen, M.S. Dargusch, J. Zou, High performance thermoelectric materials: progress and their applications, Adv. Energy Mater. 8 (2018) 1701797 https://doi.org/10.1002/aenm.201701797.
[9] H. Alam, S. Ramakrishna, A review on the enhancement of figure of merit from bulk to nano-thermoelectric materials, Nano Energy 2 (2013) 190–212 https://doi.org/10.1016/j.nanoen.2012.10.005.
[10] D.K. Ko, Y.J. Kang, C.B. Murray, Enhanced thermopower via carrier energy filtering in solution-processable Pt-Sb2Te3 nanocomposites, Nano Lett. 11 (2011) 2841–2844 https://doi.org/10.1021/nl2012246.
[11] M. He, J. Ge, Z.Q. Lin, X.H. Feng, X.W. Wang, H.B. Lu, Y.L. Yang, F. Qiu, Thermopower enhancement in conducting polymer nanocomposites via carrier energy scattering at the organic-inorganic semiconductor interface, Energy Environ. Sci. 5 (2012) 8351–8358 https://doi.org/10.1039/C2EE21803H.
[12] Y. Min, J.W. Roh, H. Yang, M. Park, S.I. Kim, S. Hwang, S.M. Lee, K.H. Lee, U. Jeong, Surfactant-free scalable synthesis of Bi2Te3 and Bi2Se3 nanoflakes and enhanced thermoelectric properties of their nanocomposites, Adv. Mater. 25 (2013) 1425–1429 https://doi.org/10.1002/adma.201203764.
[13] J. Kim, K.H. Lee, S.D. Kim, J.H. Lim, N.V. Myung, Simple and effective fabrication of Sb2Te3 films embedded with Ag2Te nanoprecipitates for enhanced thermoelectric performance, J. Mater. Chem. 6 (2018) 349–356 https://doi.org/10.1039/C7TA09013G.
[14] A.J. Minnich, M.S. Dresselhaus, Z.F. Ren, G. Chen, Bulk nanostructured thermoelectric materials: current research and future prospects, Energy Environ. Sci. 2 (2009) 466–479 https://doi.org/10.1039/b822664b.
[15] I.A. Tambasov, A.S. Voronin, N.P. Evsevskaya, M.N. Volochaev, Y.V. Fadeev, A.S. Krylov, A.S. Aleksandrovskii, A.V. Luk'yanenko, S.R. Abelyan, E.V. Tambasova, Structural and thermoelectric properties of optically transparent thin films based on single-walled carbon nanotubes, Phys. Solid State 60 (2018) 2649–2655 https://doi.org/10.1134/S1063783418120296.
[16] J.L. Blackburn, A.J. Ferguson, C. Cho, J.C. Grunlan, Carbon-nanotube-based thermoelectric materials and devices, Adv. Mater. 30 (2018) 1704386, https://doi.org/10.1002/adma.201704386.
[17] Q. Jin, S. Jiang, Y. Zhao, D. Wang, J. Qiu, D.-M. Tang, J. Tan, D.-M. Sun, P.-X. Hou, X.-Q. Chen, K. Tai, N. Gao, C. Liu, H.-M. Cheng, X. Jiang, Flexible layer-structured Bi2Te3 thermoelectric on a carbon nanotube scaffold, Nat. Mater. 18 (2019) 62–68 https://doi.org/10.1038/s41563-018-0217-z.
[18] Y. Nakai, K. Honda, K. Yanagi, H. Kataura, T. Kato, T. Yamamoto, Y. Maniwa, Giant Seebeck coefficient in semiconducting single-wall carbon nanotube film, APEX 7 (2014) 025103 https://doi.org/10.7567/Apex.7.025103.
[19] X. Mu, H.Y. Zhou, D.Q. He, W.Y. Zhao, P. Wei, W.T. Zhu, X.L. Nie, H.J. Liu, Q.J. Zhang, Enhanced electrical properties of stoichiometric Bi0.5Sb1.5Te3 film with high-crystallinity via layer-by-layer in-situ growth, Nano Energy 33 (2017) 55–64 https://doi.org/10.1016/j.nanoen.2017.01.013.
[20] C. Yang, D. Souchay, M. Kneiss, M. Bogner, M. Wei, M. Lorenz, O. Oeckler, G. Benstetter, Y.Q. Fu, M. Grundmann, Transparent flexible thermoelectric material based on non-toxic earth-abundant p-type copper iodide thin film, Nat. Commun. 8 (2017) 16076 https://doi.org/10.1038/Ncomms16076.
[21] J. Lefebvre, J. Ding, Z. Li, P. Finnie, G. Lopinski, P.R.L. Malenfant, High-purity semiconducting single-walled carbon nanotubes: a key enabling material in emerging electronics, Accounts Chem. Res. 50 (2017) 2479–2486 https://doi.org/10.1021/acs.accounts.7b00234.
[22] B.A. MacLeod, N.J. Stanton, I.E. Gould, D. Wesenberg, R. Ihly, Z.R. Owczarczyk, K.E. Hurst, C.S. Fewox, C.N. Folmar, K.H. Hughes, B.L. Zink, J.L. Blackburn, A.J. Ferguson, Large n- and p-type thermoelectric power factors from doped semiconducting single-walled carbon nanotube thin films, Energy Environ. Sci. 10 (2017) 2168–2179 https://doi.org/10.1039/C7EE01130J.
[23] A.D. Avery, B.H. Zhou, J. Lee, E.S. Lee, E.M. Miller, R. Ihly, D. Wesenberg, K.S. Mistry, S.L. Guillot, B.L. Zink, Y.H. Kim, J.L. Blackburn, A.J. Ferguson, Tailored semiconducting carbon nanotube networks with enhanced thermoelectric properties, Nat Energy 1 (2016) 16033 https://doi.org/10.1038/nenergy.2016.33.
[24] A. Chortos, I. Pochorovski, P. Lin, G. Pitner, X.Z. Yan, T.Z. Gao, J.W.F. To, T. Lei, J.W. Will, H.S.P. Wong, Z.N. Bao, Universal selective dispersion of semiconducting carbon nanotubes from commercial sources using a supramolecular polymer, ACS Nano 11 (2017) 5660–5669 https://doi.org/10.1021/acsnano.7b01076.
[25] M. Zheng, A. Jagota, M.S. Strano, A.P. Santos, P. Barone, S.G. Chou, B.A. Diner, M.S. Dresselhaus, R.S. McLean, G.B. Onoa, G.G. Samsonidze, E.D. Semke, M. Usrey, D.J. Walls, Structure-based carbon nanotube sorting by sequence-dependent DNA assembly, Science 302 (2003) 1545–1548 https://doi.org/10.1126/science.1091911.
[26] H.P. Liu, D. Nishide, T. Tanaka, H. Kataura, Large-scale single-chirality separation of single-wall carbon nanotubes by simple gel chromatography, Nat. Commun. 2 (2011) 309 https://doi.org/10.1038/ncomms1313.
[27] A.I. Chernov, E.D. Obraztsova, Metallic single-wall carbon nanotubes separated by density gradient ultracentrifugation, Physica Status Solidi B-Basic Solid State Phys. 246 (2009) 2477–2481 https://doi.org/10.1002/pssb.200982289.
[28] D. Janas, Towards monochiral carbon nanotubes: a review of progress in the sorting of single-walled carbon nanotubes, Mater. Chem. Front. 2 (2018) 36–63 https://doi.org/10.1039/C7QM00427C.
[29] J.E. Um, S.G. Song, P.J. Yoo, C. Song, W.J. Kim, Large-scale separation of single-walled carbon nanotubes by electronic type using click chemistry, Appl. Surf. Sci. 429 (2018) 278–283 https://doi.org/10.1016/j.apsusc.2017.06.092.
[30] C.Y. Khripin, J.A. Fagan, M. Zheng, Spontaneous partition of carbon nanotubes in polymer-modified aqueous phases, J. Am. Chem. Soc. 135 (2013) 6822–6825 https://doi.org/10.1021/ja402762e.
[31] V.A. Eremina, P.A. Obraztsov, P.V. Fedotov, A.I. Chernov, E.D. Obraztsova, Separation and optical identification of semiconducting and metallic single-walled carbon nanotubes, Physica Status Solidi B-Basic Solid State Phys. 254 (2017) 1600659 https://doi.org/10.1002/pssb.201600659.
[32] A.S.R. Bati, L. Yu, M. Batmunkh, J.G. Shapter, Synthesis, purification, properties and characterization of sorted single-walled carbon nanotubes, Nanoscale 10 (2018) 22087–22139 https://doi.org/10.1039/C8NR07379A.
[33] I.A. Tambasov, A.S. Tarasov, M.N. Volochaev, M.V. Rautskii, V.G. Myagkov, L.E. Bykova, V.S. Zhigalov, A.A. Matsynin, E.V. Tambasova, Weak localization and size effects in thin In2O3 films prepared by autowave oxidation, Phys. E Low-dimens. Syst. Nanostruct. 84 (2016) 162–167 https://doi.org/10.1016/j.physe.2016.06.005.
[34] V.G. Myagkov, L.E. Bykova, A.A. Matsynin, M.N. Volochaev, V.S. Zhigalov, I.A. Tambasov, Y.L. Mikhlin, D.A. Velikanov, G.N. Bondarenko, Solid state synthesis of Mn5Ge3 in Ge/Ag/Mn trilayers: structural and magnetic studies, J. Solid State Chem. 246 (2017) 379–387 https://doi.org/10.1016/j.jssc.2016.12.010.
[35] M.N. Volochaev, S.V. Komogortsev, V.G. Myagkov, L.E. Bykova, V.S. Zhigalov, N.P. Shestakov, D.A. Velikanov, D.A. Smolyakov, A.V. Luk'yanenko, V.B. Rachek, Y.Y. Loginov, I.A. Tambasov, A.A. Matsynin, Structural and magnetic characteristics of nanogranular Co–Al2O3 single- and multilayer films formed by the solid-state synthesis, Phys. Solid State 60 (2018) 1425–1431 https://doi.org/10.1134/S1063783418070302.
[36] S.M. Lee, D.G. Cahill, Heat transport in thin dielectric films, J. Appl. Phys. 81 (1997) 2590–2595 https://doi.org/10.1063/1.363923.
[37] Y.K. Koh, S.L. Singer, W. Kim, J.M.O. Zide, H. Lu, D.G. Cahill, A. Majumdar, A.C. Gossard, Comparison of the 3 omega method and time-domain thermoreflectance for measurements of the cross-plane thermal conductivity of epitaxial semiconductors, J. Appl. Phys. 105 (2009) 054303 https://doi.org/10.1063/1.3078808.
[38] D.G. Cahill, P.V. Braun, G. Chen, D.R. Clarke, S.H. Fan, K.E. Goodson, P. Keblinski, W.P. King, G.D. Mahan, A. Majumdar, H.J. Maris, S.R. Phillpot, E. Pop, L. Shi, Nanoscale thermal transport. II. 2003-2012, Appl. Phys. Rev. 1 (2014) 011305 https://doi.org/10.1063/1.4832615.
[39] D.G. Cahill, Thermal-conductivity measurement from 30-K to 750-K - the 3-omega method, Rev. Sci. Instrum. 61 (1990) 802–808 https://doi.org/10.1063/1.1141498.
[40] W. Huang, E. Tokunaga, Y. Nakashima, T. Fujigaya, Thermoelectric properties of sorted semiconducting single-walled carbon nanotube sheets, Sci. Technol. Adv. Mater. 20 (2019) 97–104 https://doi.org/10.1080/14686996.2019.1567107.
[41] A.A. Ivanenko, I.A. Tambasov, A.A. Pshenichnaia, N.P. Shestakov, Flexible film broadband absorber based on diamond-graphite mixture and polyethylene, Opt. Mater. 73 (2017) 388–392 https://doi.org/10.1016/j.optmat.2017.08.041.
[42] K. Mizuno, J. Ishii, H. Kishida, Y. Hayamizu, S. Yasuda, D.N. Futaba, M. Yumura, K. Hata, A black body absorber from vertically aligned single-walled carbon

nanotubes, Proc. Natl. Acad. Sci. USA 106 (2009) 6044–6047 https://doi.org/10.1073/pnas.0900155106.
[43] B. Norton-Baker, R. Ihly, I.E. Gould, A.D. Avery, Z.R. Owczarczyk, A.J. Ferguson, J.L. Blackburn, Polymer-free carbon nanotube thermoelectrics with improved charge carrier transport and power factor, ACS Energy Lett. 1 (2016) 1212–1220 https://doi.org/10.1021/acsenergylett.6b00417.
[44] M. Burghard, Electronic and vibrational properties of chemically modified single-wall carbon nanotubes, Surf. Sci. Rep. 58 (2005) 1–109 https://doi.org/10.1016/j.surfrep.2005.07.001.
[45] S. Azoubel, S. Magdassi, Controlling adhesion properties of SWCNT-PET films prepared by wet deposition, ACS Appl. Mater. Interfaces 6 (2014) 9265–9271 https://doi.org/10.1021/am501488p.
[46] C.Y. Su, A.Y. Lu, Y.L. Chen, C.Y. Wei, P.C. Wang, C.H. Tsai, Chemically-treated single-walled carbon nanotubes as digitated penetrating electrodes in organic solar cells, J. Mater. Chem. 20 (2010) 7034–7042 https://doi.org/10.1039/C0JM00578A.
[47] L.B. Hu, D.S. Hecht, G. Gruner, Carbon nanotube thin films: fabrication, properties, and applications, Chem. Rev. 110 (2010) 5790–5844 https://doi.org/10.1021/cr9002962.
[48] M.E. Itkis, F. Borondics, A.P. Yu, R.C. Haddon, Bolometric infrared photoresponse of suspended single-walled carbon nanotube films, Science 312 (2006) 413–416 https://doi.org/10.1126/science.1125695.
[49] T.J. Kang, T. Kim, S.M. Seo, Y.J. Park, Y.H. Kim, Thickness-dependent thermal resistance of a transparent glass heater with a single-walled carbon nanotube coating, Carbon 49 (2011) 1087–1093 https://doi.org/10.1016/j.carbon.2010.11.012.
[50] D. Kim, H.C. Lee, J.Y. Woo, C.S. Han, Thermal behavior of transparent film heaters made of single-walled carbon nanotubes, J. Phys. Chem. C 114 (2010) 5817–5821 https://doi.org/10.1021/jp910799a.
[51] S. Mouri, Y. Miyauchi, K. Matsuda, Dispersion-process effects on the photoluminescence quantum yields of single-walled carbon nanotubes dispersed using aromatic polymers, J. Phys. Chem. C 116 (2012) 10282–10286 https://doi.org/10.1021/jp212040y.
[52] A.V. Naumov, D.A. Tsyboulski, S.M. Bachilo, R.B. Weisman, Length-dependent optical properties of single-walled carbon nanotube samples, Chem. Phys. 422 (2013) 255–263 https://doi.org/10.1016/j.chemphys.2012.12.033.
[53] B. Kumanek, D. Janas, Thermal conductivity of carbon nanotube networks: a review, J. Mater. Sci. (2019) 7397–7427 https://doi.org/10.1007/s10853-019-03368-0.